



Transmit antenna selection for millimeter-wave communications using multi-RIS with imperfect transceiver hardware

Nguyen Van Vinh¹

Accepted: 12 April 2024

© The Author(s), under exclusive licence to Springer Science+Business Media, LLC, part of Springer Nature 2024

Abstract

This article presents a comprehensive exploration of the synergy between transmit antenna selection (TAS) and reconfigurable intelligent surfaces (RISs) in millimeter-wave (MW) communication systems, considering the impact of practical conditions. Notably, it accounts for imperfect transceiver hardware (ITH) at both the transmitter and receiver. Additionally, real-world channel models and receiver noise statistics are integrated into the analysis, providing a realistic representation of wireless systems in future networks. Mathematical formulas of outage probability (OP) and system throughput (ST) of the multi-RIS-assisted MW communications with ITH and TAS (shortened as the considered communications) are derived for analyzing the system behaviors. These formulas facilitate a comprehensive examination of system behavior. Through a series of comparative scenarios, including evaluations of OP and ST with and without TAS, with and without RISs, and with and without ITH (where the absence of ITH is denoted as perfect transceiver hardware, or PTH), the study substantiates the substantial advantages of TAS and RISs while shedding light on the significant influence of ITH. It is demonstrated that even in the presence of ITH, MW communication performance can be dramatically enhanced by optimizing the number of transmit antennas, selecting suitable carrier frequencies and RIS placements, and utilizing appropriate bandwidth. Ultimately, the derived formulas are rigorously validated through Monte-Carlo simulations, reinforcing the credibility of the findings.

Keywords Transmit antenna selection · Reconfigurable intelligent surfaces · Millimeter-wave communications · Performance metrics · Moment functions

1 Introduction

Indeed, it has been substantiated that transmit antenna selection (TAS) serves as an effective solution for significantly reducing signal processing complexity and markedly improving the performance of multiple-input multiple-output systems [1]. Because of its advantages, TAS was widely used in the previous generations of mobile communications (3G & 4G) and it is being an effective method to use in the future generations (5G & B5G) [1, 2]. In particular, a transmit antenna is chosen from N antennas to dramatically enhance the received power. Consequently, the effects of the negative parameters, e.g., residual self-interference and imperfect transceiver hardware (ITH) can be indirectly reduced [2]. Therefore, TAS becomes an effective manner

with low cost and low computational complexity for applying in 5G & B5G networks [3].

On the other hand, 5G & B5G networks exploit the high carrier frequencies of millimeter-wave (MW) bands. Therefore, the number of antennas at wireless nodes can be considerably extended [4]. Specifically, MW communications operate within a wavelength range spanning from 1 to 10 mm, corresponding to carrier frequencies that range from 30 to 300 GHz. This extensive bandwidth allows for the deployment of numerous antennas in wireless nodes that operate within the MW bands [4–18]. As a result, the data speeds of MW communications can be significantly increased. However, the main disadvantage of MW communications is that they are strongly affected by blockages [5]. Thus, many solutions such as TAS, beamforming, and channel estimation have been applied to reduce the effects caused by the elevated carrier frequencies inherent to MW bands. [19].

✉ Nguyen Van Vinh
vinhvn27@fe.edu.vn

¹ Department of Information Assurance (IA), FPT University,
Ha Noi, Vietnam

Table 1 Comparison with the existing works

Paper	Channel	Devices	Hardware	Metrics (values)
[29]	Rayleigh	A RIS	PTH	Capacity (0.8 bit/s/Hz)
[30]	Rayleigh	A RIS	PTH	Capacity (0.5 bit/s/Hz), error probability (10^{-5})
[36]	Rayleigh	Multi-RIS	PTH	Capacity (25 bit/s/Hz)
[39]	Rayleigh	A RIS	PTH	Energy efficient (20 bit/J/Hz)
[43]	Rayleigh	No RIS	PTH	OP (10^{-3}), ST (4 bit/s/Hz)
[44]	Nakagami	Multi-RIS	PTH	OP (10^{-8})
[51]	Nakagami	Multi-RIS	ITH	OP (10^{-4}), ST (4 bit/s/Hz)
[54]	Rayleigh	A RIS	PTH	OP (10^{-5}), capacity (20 bit/s/Hz)
[55]	Rayleigh	A RIS	ITH	OP (10^{-2}), Capacity (12 bit/s/Hz)
[56]	Rayleigh	A RIS	PTH	OP (10^{-3})
This paper	Nakagami and 5G/B5G standards	Multi-RIS	ITH	OP, ST with TAS

1.1 Related works

To exploit the benefits of utilizing high carrier frequencies, many new techniques such as reconfigurable intelligent surface (RIS), full-duplex, and unmanned aerial vehicle have been studied and combined in MW communications [4, 19–22]. More specifically, RIS technology has recently emerged as a powerful paradigm for applying in B5G networks [23, 24]. In particular, RIS is made from metasurfaces that can effectively reflect wireless signals without power supply, processor, converter, and amplifier [25–28]. Therefore, compared with traditional relays, the usage of advanced RIS in wireless communications can achieve many benefits, especially with larger sizes of RIS or bigger numbers of reflecting elements (REs) [29–32]. Moreover, the RIS can be deployed at the top of factories/buildings, thus, the effects caused by blockages in MW communications may be greatly reduced [33–35]. Besides one-RIS, multi-RIS was also utilized in MW communications [36, 37].

In recent reports, TAS has been utilized in multi-RIS-assisted MW communications [37]. In this TAS scheme, only one transmit antenna is selected from N transmit antennas based on link power to maximize the received power at the receiver/user. As a result, by utilizing TAS, the received power is much increased while the computational complexity is significantly reduced in comparison with the case that either several transmit antennas or all transmit antennas are active [2, 37–42]. Importantly, the system performance using TAS can keep as close to alternative solutions as possible [43]. In particular, by exploiting multi-antenna at base station, the outage probability (OP) and system throughput (ST) of MW communications are greatly enhanced. Thus, the effects of negative parameters in the systems can be significantly reduced.

Moreover, the signal processing complexity at the mobile user is also decreased. However, a practical condition, i.e., ITH was often neglected [37, 44–46]. In the meanwhile, it has been demonstrated that ITH always exists in wireless communications because of hardware characteristics [47, 48]. In particular, ITH can be found in electronic components, especially in cost-effective devices. More specifically, ITH is influenced by disparities in in-phase/quadrature components, phase noise, and the nonlinearity of converters (both analog-to-digital and digital-to-analog), mixers, and amplifiers. These components encompass high-power amplifiers in transmitters and low-noise amplifiers in receivers [47, 49–51]. These imperfections often lead to discrepancies between intended and actual signals [49–51]. Several methods have been proposed to address these limitations in both analog and digital domains [47, 48, 50, 51]. Nonetheless, residual impairments stemming from inherent electronic component defects, imperfect parameter estimation of variable hardware characteristics, limitations in precision models, and basic compensation algorithms prevent complete elimination of distortion noises. Additionally, these impairments vary over time as they present new manifestations for each fresh data signal [48, 51]. Utilizing the central limit theorem and experimental observations, the cumulative impact of numerous impairments can be characterized by complex Gaussian variables [48–53]. Consequently, neglecting ITH when assessing the performance of wireless communications can result in erroneous or imprecise conclusions [49]. In addition, it was demonstrated that the ITH has a great effect on the performance of RIS-assisted wireless communications [50–53]. For improved readability, we provide a summary of existing works in Table 1. Please note that the performance metric values are evaluated at a transmit power of 30 dBm.

1.2 Motivation and contributions

As the above discussions, the huge advantages of TAS and multi-RIS have been confirmed in the literature. However, only one RIS was often used to assist MW communications in the previous works [19, 57]. Moreover, exploiting both TAS and multi-RIS in MW communications is still lacking, except for the work in [37]. Unfortunately, [37] considered the case of perfect transceiver hardware (PTH). The case of ITH was not studied yet. Meanwhile, ignoring ITH can result in some inaccuracies into the system behaviors. It is because the transceiver hardware is varied and belongs to the intrinsic properties of electronic components, especially the random and time varying hardware characteristics [50, 51]. Motivated from these facts, in this article, the benefits of TAS and multi-RIS are combined in the MW communications with ITH. More specifically, by utilizing TAS and RISs, the negative effects of ITH are greatly reduced. It is because the received signal-to-noise ratio (SNR) at the receiver will be dramatically increased with TAS and RISs. As a result, the received SNR with TAS and RISs is significantly higher than that without TAS and without RISs. The mathematical formulas of OP and ST of the considered communications (the multi-RIS-assisted MW communications with ITH and with TAS) are derived and then compared with those of the relevant communications (the MW communications without RISs, with PTH, and without TAS)¹. From the acquired findings and observed behaviors of the multi-RIS-assisted MW communications with ITH and with TAS, the potential for broadening the scope of the considered communications becomes apparent, encompassing comprehensive models featuring multi-RIS configurations, multiple antennas, and multiple relays within the domain of MW communications, adaptable to diverse scenarios. Notably, the considered multi-RIS-assisted MW communications with ITH and with TAS along with their extensions exhibit suitability for integration into sensor systems and internet of things (IoT) networks, particularly well-suited for operation in specialized environments such as disaster-stricken areas, mountainous terrains, and wooded areas. In these circumstances, establishing a reliable power supply for communication nodes proves arduous, leading to insufficient power reserves for extensive and prolonged communication over extended distances. As a result, employing strategies such as multi-hop relaying, multi-RIS deployment, and multi-antenna architectures emerges as effective solutions. The

¹ It is noteworthy that while mathematical analysis provides valuable insights into the behavior of wireless communication systems, it is essential to recognize its limitations in capturing the full complexity of real-world scenarios. Integrating simulations, empirical studies, and practical experiments is often necessary to complement mathematical models and obtain a more comprehensive understanding of wireless communication systems.

incorporation of RISs holds particular promise as it significantly amplifies coverage and substantially curtails energy consumption because the RISs can reflect signals without a power supply. The main contributions of this article can be shortened as follows:

- A practical scenario is considered where ITH is taken into investigation of multi-RIS-assisted MW communications. Besides ITH, the path loss models and receiver noise are also measured based on practical deployments of 5 G & B5G networks. Consequently, the multi-RIS-assisted MW communications with ITH can comprehensively reflect the behaviors of 5 G & B5G networks deployed in practice. To significantly reduce the negative effects of ITH and other parameters, TAS is utilized at the base station.
- The mathematical formulas of OP and ST of the multi-RIS-assisted MW communications with TAS are derived under the effects of ITH. We observe that mathematical derivations are challenging with ITH. Consequently, the computational complexity is significantly higher than that of previous works [37, 50, 54]. Hence, the derived equations are notably more intricate compared to those presented in prior studies [37, 50, 54, 55]. From the derived formulas, it's easy to obtain the other formulas of relevant communications such as MW communications with and without RISs in the cases of without TAS and with ITH, with TAS and with PTH, and without TAS and with PTH. Monte-Carlo simulation results are conducted to verify the exactness of the derived formulas.
- The OP and ST of the considered MW communications (with ITH, with RISs, and with TAS) are evaluated and compared with those of MW communications in the cases with PTH, without RISs, and without TAS. Through many compared scenarios presented in numerical results, the great effects of ITH are detailedly analyzed. In this circumstance, the usage of TAS and multiple RISs are effective solutions. Specifically, besides the separate benefits of TAS and RISs, the joint benefits of them are also confirmed. Specifically, with a certain condition, the OP and ST performances with TAS are considerably higher than the OP and ST performances without TAS. Similarly, the performances with RISs are dramatically higher than those without RISs. From the communication behaviors, many solutions such as using larger number of transmit antennas, utilizing suitable carrier frequencies and bandwidths, and locating RISs in appropriate areas can be utilized for significantly reducing the OP and increasing ST of the considered communications.

The rest of this article follows this structure: Sect. 2 introduces the system model and the signal formulas relevant to

Table 2 Mathematical notations

Notation	Description
l^{th}/k^{th}	The k^{th} RE of the l^{th} RIS
G_l	Number of REs of the l^{th} RIS
$\mathbb{E}\{.\}$	Expectation operator
$\Pr\{.\}$	Probability operator
$F(.)$	Cumulative distribution function (CDF)
$\Gamma(.,.)$	Upper incomplete gamma function
$\gamma(.,.)$	Lower incomplete Gamma function
$f(.)$	Probability density function (PDF)
$\mathcal{K}_u(.)$	The u^{th} order modified Bessel function of the second kind
$\Gamma(.)$	Gamma function

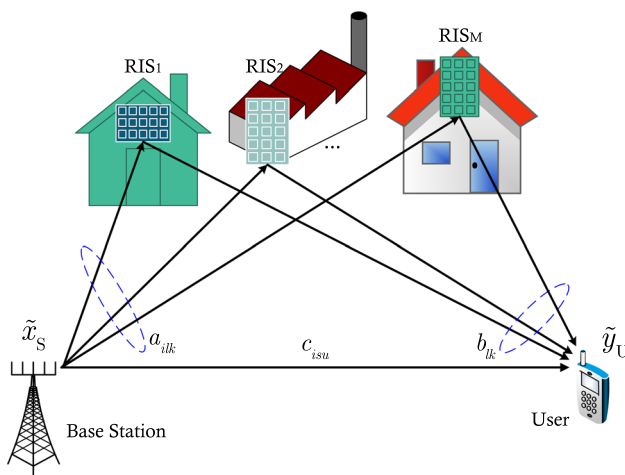


Fig. 1 Illustration of the multi-RIS-assisted MW communications with ITH

the communication under consideration. Section 3 detailedly analyzes the communication performance by deriving the OP and ST formulas with ITH and with TAS. Section 4 illustrates the communication behaviors under the effects of system parameters. In conclusion, Sect. 5 provides the final remarks and conclusions for this article. For ease of reading, the mathematical notations are included in Table 2.

2 System model

The block diagram of the multi-RIS-assisted MW communications with ITH is plotted in Fig. 1. In particular, the considered communications consist of three components, i.e., a base station (S), M RISs, and a user (U). Since the wavelengths in the MW communications are utilized, S includes N transmit antennas. Meanwhile, U is a personal device, it is

equipped with only one receive antenna.² M RISs are distributed in different areas, where the l^{th} RIS ($l = 1, 2, \dots, M$) has G_l REs.³ In the case of PTH, the transmit signal at S and the received signal at U are, respectively, x_S and y_U . Meanwhile, in the case of ITH, they are, respectively, \tilde{x}_S and \tilde{y}_U . Herein, \tilde{x}_S includes an ITH component of the transmitter S while \tilde{y}_U consists of the ITH components of both the transmitter S and receiver U. Since the RISs are expected to deploy in B5G networks, besides the S-RIS-U links, the considered model comprises the classical S-U link that has been often exploited in 3 G/4 G/5 G networks.

At every transmission time slot, TAS is utilized at S. Thus, S selects one antenna (denoted by the i^{th} antenna in the followings) from N transmit antennas for transmitting signal to U. The received signal at U with ITH can be formulated as

$$\tilde{y}_U = \left(\sum_{l=1}^M \sum_{k=1}^{G_l} a_{ilk} b_{lk} \exp(j\varphi_{lk}) + c_{isu} \right) (x_S + n_S^t) + n_U^r + z_U, \tag{1}$$

where a_{ilk} and c_{isu} are the channels from the i^{th} antenna of S to the l^{th}/k^{th} and to U, respectively; b_{lk} is the channel from the l^{th}/k^{th} to U; φ_{lk} is the phase shift induced by the l^{th}/k^{th} ; x_S and n_S^t denote the desired signal and distortion noise induced by ITH of transmitter S, respectively; n_U^r is distortion noise induced by ITH of receiver U; z_U is the Gaussian noise at U, i.e., $z_U \sim \mathcal{CN}(0, \sigma_U^2)$.

It is because a_{ilk} , c_{isu} , and b_{lk} are complex numbers, they can be represented as $a_{ilk} = \bar{a}_{ilk} \exp(-j\phi_{ilk})$, $c_{isu} = \bar{c}_{isu} \exp(-j\theta_{isu})$, and $b_{lk} = \bar{b}_{lk} \exp(-j\psi_{lk})$, where \bar{a}_{ilk} , \bar{c}_{isu} , and \bar{b}_{lk} are the magnitudes and ϕ_{ilk} , θ_{isu} , and ψ_{lk} are the phases of a_{ilk} , c_{isu} , and b_{lk} , respectively. On the other hand, a phase matrix is often used to express the phases of the l^{th} RIS, e.g.,

$$\Psi_l = \text{diag} \left(\exp(j\varphi_{l1}), \dots, \exp(j\varphi_{lk}), \dots, \exp(j\varphi_{lG_l}) \right). \tag{2}$$

Based on the magnitudes and phases of a_{ilk} , c_{isu} , and b_{lk} , (1) is represented as

² Based on the system characteristics used in 5G and B5G networks, S can use patch array antennas while U can use sector, log-periodic, and/or patch antenna [7–11, 58].

³ Notice that RISs can be implemented using either passive or active elements. These surfaces are designed to enhance wireless communication systems by manipulating the propagation environment. The choice between passive and active RIS depends on various factors such as the specific application, energy constraints, system requirements, and cost considerations. Passive RIS may be suitable for static environments or applications where energy efficiency is critical, while active RIS provides greater flexibility and adaptability in dynamic scenarios. Based on these observations, we use passive RISs in our work [34, 35, 59].

$$\begin{aligned} \tilde{y}_U &= \left(\sum_{l=1}^M \sum_{k=1}^{G_l} \bar{a}_{ilk} \bar{b}_{lk} \exp(j\varphi_{lk} - j\phi_{ilk} - j\psi_{lk}) \right. \\ &\quad \left. + \bar{c}_{isu} \exp(-j\theta_{isu}) \right) (x_S + n_S^t) + n_U^r + z_U \\ &= \exp(-j\theta_{isu}) \left(\sum_{l=1}^M \sum_{k=1}^{G_l} \bar{a}_{ilk} \bar{b}_{lk} \exp(j\varphi_{lk} + j\theta_{isu} - j\phi_{ilk} - j\psi_{lk}) \right. \\ &\quad \left. + \bar{c}_{isu} \right) (x_S + n_S^t) + n_U^r + z_U. \end{aligned} \tag{3}$$

Then, (3) is reorganized as

$$\tilde{y}_U = \exp(-j\theta_{isu}) \left(\sum_{l=1}^M \sum_{k=1}^{G_l} \bar{a}_{ilk} \bar{b}_{lk} \exp(j\xi_{lk}) + \bar{c}_{isu} \right) (x_S + n_S^t) + n_U^r + z_U, \tag{4}$$

where $\xi_{lk} = \varphi_{lk} + \theta_{isu} - \phi_{ilk} - \psi_{lk}$.

As confirmed in the literature, one of the RISs' advantages is that their phases can be adjusted independently [33, 51]. Specifically, due to the features of metasurfaces that are used to make RISs, the RISs' phases are independently tuned [19]. Also, each RIS is controlled by a smart controller with communication-oriented software. In addition, the RISs' phases are discrete because of hardware conditions [60]. As a result, with the smart controller, communication-oriented software, discrete phases, and perfect channel estimation, an expected phase can be picked up from a discrete phase set to generate $\xi_{lk} = 0$ for all l and k [19, 24, 33, 51]. In other words, we have $\varphi_{lk} + \theta_{isu} - \phi_{ilk} - \psi_{lk} = 0$. Consequently, the phase φ_{lk} of the l^{th}/k^{th} is chosen as

$$\varphi_{lk} = \phi_{ilk} + \psi_{lk} - \theta_{isu}. \tag{5}$$

After picking up the ideal/optimal phase, the received signal at U from (4) becomes

$$\tilde{y}_U = \exp(-j\theta_{isu}) \left(\sum_{l=1}^M \sum_{k=1}^{G_l} \bar{a}_{ilk} \bar{b}_{lk} + \bar{c}_{isu} \right) (x_S + n_S^t) + n_U^r + z_U. \tag{6}$$

It is noteworthy that the distortion noises induced by ITH can be expressed as [50, 51] $n_S^t \sim \mathcal{CN}(0, (\alpha_S^t)^2 P_S)$ and

$n_U^r \sim \mathcal{CN}(0, |\exp(-j\theta_{isu}) (\sum_{l=1}^M \sum_{k=1}^{G_l} \bar{a}_{ilk} \bar{b}_{lk} + \bar{c}_{isu})|^2 (\alpha_U^r)^2 P_S)$, where $P_S = \mathbb{E}\{|x_S|^2\}$; α_S^t and α_U^r denote the ITH levels at transmitter S and receiver U, respectively.

For convenience in observation, (6) is now represented as

$$\begin{aligned} \tilde{y}_U &= \underbrace{\exp(-j\theta_{isu}) \left(\sum_{l=1}^M \sum_{k=1}^{G_l} \bar{a}_{ilk} \bar{b}_{lk} + \bar{c}_{isu} \right) x_S + z_U}_{\mathcal{I}} \\ &\quad + \underbrace{\exp(-j\theta_{isu}) \left(\sum_{l=1}^M \sum_{k=1}^{G_l} \bar{a}_{ilk} \bar{b}_{lk} + \bar{c}_{isu} \right) n_S^t + n_U^r}_{\mathcal{J}}. \end{aligned} \tag{7}$$

It is obvious from (7) that the term \mathcal{I} presents the received signal at U with PTH while the term \mathcal{J} is the distortion noise induced by ITH. In other words, when the ideal hardware is considered in the RISs-assisted wireless communications [19, 33], the term \mathcal{J} is set as $\mathcal{J} = 0$.

Based on the above definitions of the distortion noises, the total distortion noise power at U can be formulated as

$$\begin{aligned} &\mathbb{E} \left\{ \left| \exp(-j\theta_{isu}) \left(\sum_{l=1}^M \sum_{k=1}^{G_l} \bar{a}_{ilk} \bar{b}_{lk} + \bar{c}_{isu} \right) n_S^t + n_U^r \right|^2 \right\} \\ &= \left| \exp(-j\theta_{isu}) \left(\sum_{l=1}^M \sum_{k=1}^{G_l} \bar{a}_{ilk} \bar{b}_{lk} + \bar{c}_{isu} \right) \right|^2 \left[(\alpha_S^t)^2 P_S + (\alpha_U^r)^2 P_S \right]. \end{aligned} \tag{8}$$

Then, the signal-to-distortion-plus-noise ratio (SDNR) at U calculated from (7) is

$$\rho_U = \frac{\left| \exp(-j\theta_{isu}) \left(\sum_{l=1}^M \sum_{k=1}^{G_l} \bar{a}_{ilk} \bar{b}_{lk} + \bar{c}_{isu} \right) \right|^2 P_S}{\mathbb{E} \left\{ \left| \exp(-j\theta_{isu}) \left(\sum_{l=1}^M \sum_{k=1}^{G_l} \bar{a}_{ilk} \bar{b}_{lk} + \bar{c}_{isu} \right) n_S^t + n_U^r \right|^2 \right\} + \sigma_U^2}. \tag{9}$$

Utilizing (8) combining with the property $|\exp(-j\theta_{isu})|^2 = 1$, (9) now becomes⁴

$$\rho_U = \frac{\left(\sum_{l=1}^M \sum_{k=1}^{G_l} \bar{a}_{ilk} \bar{b}_{lk} + \bar{c}_{isu} \right)^2 P_S}{\left(\sum_{l=1}^M \sum_{k=1}^{G_l} \bar{a}_{ilk} \bar{b}_{lk} + \bar{c}_{isu} \right)^2 \left[(\alpha_S^t)^2 + (\alpha_U^r)^2 \right] P_S + \sigma_U^2}. \tag{10}$$

On the other hand, we would like to take our considered communications practically. Thus, besides ITH, we also consider the noise power based on practical receivers [61], e.g.,

$$\sigma_U^2 = N_0 + N_F + 10 \log(B_W), \tag{11}$$

where N_0 is the thermal noise power density; N_F is the noise figure; B_W is the bandwidth. We should note that prior researches often normalized the noise power by setting $\sigma_U^2 = 1$ [19, 33, 56]. Consequently, their results cannot fully reflect the impacts of N_0 , N_F , and B_W on the RISs-assisted wireless communication performance.

⁴ Due to the existence of term $\left(\sum_{l=1}^M \sum_{k=1}^{G_l} \bar{a}_{ilk} \bar{b}_{lk} + \bar{c}_{isu} \right)^2 \left[(\alpha_S^t)^2 + (\alpha_U^r)^2 \right] P_S$ in denominator of (10), it is challenging to calculate OP and throughput of the considered communications. However, it is important to consider the case with ITH because of its practical characteristics in wireless communications.

3 Performance analysis

In this section, the OP and ST formulas of the considered communications are derived over Nakagami- m channels. Because of Nakagami- m environments, the channel magnitudes are subject to Gamma distribution with the shape (denoted by m) and spread (denoted by Ω) parameters. In the following, (m_{a_l}, Ω_{a_l}) , (m_{b_l}, Ω_{b_l}) , and (m_{su}, Ω_{su}) are, respectively, the channel parameters of S- l^{th} , l^{th} -U, and S-U channels. Furthermore, the channel magnitude characteristics can be expressed via their CDF and PDF using m and Ω . For example, the CDF ($F(\cdot)$) and PDF ($f(\cdot)$) of \bar{a}_{lk} are, respectively, given as [62]

$$F_{\bar{a}_{lk}}(\rho) = \frac{1}{\Gamma(m_{a_l})} \gamma(m_{a_l}, \frac{m_{a_l}}{\Omega_{a_l}} \rho^2) = 1 - \frac{1}{\Gamma(m_{a_l})} \Gamma(m_{a_l}, \frac{m_{a_l}}{\Omega_{a_l}} \rho^2), \rho \geq 0, \tag{12}$$

$$f_{\bar{a}_{lk}}(\rho) = \frac{2m_{a_l}}{\Gamma(m_{a_l})\Omega_{a_l}^{m_{a_l}}} \rho^{2m_{a_l}-1} \exp(-\frac{m_{a_l}}{\Omega_{a_l}} \rho^2), \rho \geq 0. \tag{13}$$

On the other hand, unlike the previous works where Ω is often normalized, e.g., $\Omega = 1$ [19, 33, 56], in the considered communications, Ω is computed via transmitter-receiver distance (d), carrier frequency (f_c), transmitter and receiver antenna gains (G_{tx} & G_{rx}), and environmental characteristics. More specifically, Ω in the case of non-light-of-sight (NLoS) is formulated as⁵ [63]

$$\Omega = -31.7 \log(d) - 20 \log(f_c) + G_{\text{tx}} + G_{\text{rx}} - 32.4. \tag{14}$$

Note that the values of path losses depend on the specific distances between S and RISs, RISs and U. Consequently, when the S-RISs and RISs-U distances are different, Ω_{a_l} and Ω_{b_l} will be different.

3.1 Outage probability

The OP of the considered communications with TAS is formulated as

$$\mathcal{P}_{\text{out}} = \Pr\{\rho_U < \rho_{\text{th}}\}, \tag{15}$$

where ρ_U is the SDNR of the considered communications with TAS that is given in (10); $\rho_{\text{th}} = 2^{\mathcal{R}} - 1$ is defined as the SDNR threshold. Herein, \mathcal{R} is the required rate of the considered communications calculated in bits per channel use (bpcu).

Substituting ρ_U in (10) into (15), the OP is then formulated as

$$\mathcal{P}_{\text{out}} = \Pr\left\{ \frac{\left(\sum_{l=1}^M \sum_{k=1}^{G_l} \bar{a}_{ilk} \bar{b}_{lk} + \bar{c}_{isu}\right)^2 P_S}{\left(\sum_{l=1}^M \sum_{k=1}^{G_l} \bar{a}_{ilk} \bar{b}_{lk} + \bar{c}_{isu}\right)^2 \left[(\alpha_S^t)^2 + (\alpha_U^r)^2\right] P_S + \sigma_U^2} < \rho_{\text{th}} \right\}. \tag{16}$$

Then, (16) is reorganized as

$$\mathcal{P}_{\text{out}} = \Pr\left\{ \left(\sum_{l=1}^M \sum_{k=1}^{G_l} \bar{a}_{ilk} \bar{b}_{lk} + \bar{c}_{isu}\right)^2 \left(1 - [(\alpha_S^t)^2 + (\alpha_U^r)^2] \rho_{\text{th}}\right) P_S < \sigma_U^2 \rho_{\text{th}} \right\}. \tag{17}$$

It is clear from (17) that when $1 - [(\alpha_S^t)^2 + (\alpha_U^r)^2] \rho_{\text{th}} \leq 0$, this probability is always true. It is because the left term, $\left(\sum_{l=1}^M \sum_{k=1}^{G_l} \bar{a}_{ilk} \bar{b}_{lk} + \bar{c}_{isu}\right)^2 \left(1 - [(\alpha_S^t)^2 + (\alpha_U^r)^2] \rho_{\text{th}}\right) P_S$, is either less than or equal to zero while the right term, $\sigma_U^2 \rho_{\text{th}}$, is greater than zero. In other words, $\mathcal{P}_{\text{out}} = 1$ when $1 - [(\alpha_S^t)^2 + (\alpha_U^r)^2] \rho_{\text{th}} \leq 0$.

When $1 - [(\alpha_S^t)^2 + (\alpha_U^r)^2] \rho_{\text{th}} > 0$, (17) is equivalent to

$$\mathcal{P}_{\text{out}} = \Pr\left\{ \left(\sum_{l=1}^M \sum_{k=1}^{G_l} \bar{a}_{ilk} \bar{b}_{lk} + \bar{c}_{isu}\right)^2 < \frac{\sigma_U^2 \rho_{\text{th}}}{\left(1 - [(\alpha_S^t)^2 + (\alpha_U^r)^2] \rho_{\text{th}}\right) P_S} \right\}. \tag{18}$$

Since S applies TAS scheme, the channel magnitudes are subject to the condition in (19), i.e.,

$$\begin{aligned} & \sum_{l=1}^M \sum_{k=1}^{G_l} \bar{a}_{ilk} \bar{b}_{lk} + \bar{c}_{isu} \\ &= \max \left(\sum_{l=1}^M \sum_{k=1}^{G_l} \bar{a}_{1lk} \bar{b}_{lk} + \bar{c}_{1su}, \sum_{l=1}^M \sum_{k=1}^{G_l} \bar{a}_{2lk} \bar{b}_{lk} + \bar{c}_{2su}, \dots, \sum_{l=1}^M \sum_{k=1}^{G_l} \bar{a}_{Nlk} \bar{b}_{lk} + \bar{c}_{Nsu} \right). \end{aligned} \tag{19}$$

As a result, (18) is equivalent to

$$\begin{aligned} \mathcal{P}_{\text{out}} = & \Pr\left\{ \left(\sum_{l=1}^M \sum_{k=1}^{G_l} \bar{a}_{1lk} \bar{b}_{lk} + \bar{c}_{1su}\right)^2 < \frac{\sigma_U^2 \rho_{\text{th}}}{\left(1 - [(\alpha_S^t)^2 + (\alpha_U^r)^2] \rho_{\text{th}}\right) P_S} \right\} \\ & \cup \Pr\left\{ \left(\sum_{l=1}^M \sum_{k=1}^{G_l} \bar{a}_{2lk} \bar{b}_{lk} + \bar{c}_{2su}\right)^2 < \frac{\sigma_U^2 \rho_{\text{th}}}{\left(1 - [(\alpha_S^t)^2 + (\alpha_U^r)^2] \rho_{\text{th}}\right) P_S} \right\} \cup \dots \\ & \cup \Pr\left\{ \left(\sum_{l=1}^M \sum_{k=1}^{G_l} \bar{a}_{Nlk} \bar{b}_{lk} + \bar{c}_{Nsu}\right)^2 < \frac{\sigma_U^2 \rho_{\text{th}}}{\left(1 - [(\alpha_S^t)^2 + (\alpha_U^r)^2] \rho_{\text{th}}\right) P_S} \right\}. \end{aligned} \tag{20}$$

Since

$$\begin{aligned} \mathbb{E}\left\{ \left(\sum_{l=1}^M \sum_{k=1}^{G_l} \bar{a}_{1lk} \bar{b}_{lk} + \bar{c}_{1su}\right)^2 \right\} &= \mathbb{E}\left\{ \left(\sum_{l=1}^M \sum_{k=1}^{G_l} \bar{a}_{2lk} \bar{b}_{lk} + \bar{c}_{2su}\right)^2 \right\} = \dots \\ &= \mathbb{E}\left\{ \left(\sum_{l=1}^M \sum_{k=1}^{G_l} \bar{a}_{Nlk} \bar{b}_{lk} + \bar{c}_{Nsu}\right)^2 \right\}, \end{aligned} \tag{21}$$

\mathcal{P}_{out} in (20) can be straightforwardly obtained when only one probability in (20) is solved. As a result, (20) is equivalent to

⁵ In the case of light-of-sight (LoS), Ω is calculated as $\Omega = -21 \log(d) - 20 \log(f_c) + G_{\text{tx}} + G_{\text{rx}} - 32.4$.

Table 3 The notations used in the figures

Communication characteristics	Notations
With ITH, with RISs, and with TAS	I-Wi-R & Wi-T
With PTH, with RISs, and with TAS	P-Wi-R & Wi-T
With ITH, with RISs, and without TAS	I-Wi-R & Wo-T
With PTH, with RISs, and without TAS	P-Wi-R & Wo-T
With ITH, without RISs, and with TAS	I-Wo-R & Wi-T
With PTH, without RISs, and with TAS	P-Wo-R & Wi-T
With ITH, without RISs, and without TAS	I-Wo-R & Wo-T
With PTH, without RISs, and without TAS	P-Wo-R & Wo-T

Table 4 Parameter settings

Parameters	Values
Number of RISs, M	3
Shape parameter, m	2
Thermal noise power density, N_0 [dBm/Hz]	-174
Noise figure, N_f [dBm]	10
Antenna gains, G_{tx}, G_{rx} [dB]	5
Carrier frequency, f_c [GHz]	30, 50, 70
Position of S, (\hat{x}_S, \hat{y}_S)	(0, 20)
Position of U, (\hat{x}_U, \hat{y}_U)	(100, 2)
x-axes of RISs, \mathbf{x}_{RISs}	10, 20, 40, 50, 60, 90
y-axes of RISs, \mathbf{y}_{RISs}	5, 10, 15
Transmit power, P_S [dBm]	0 ~ 60
Number of REs, G_l	50
ITH level, α^2	0 ~ 0.3
Required rate, \mathcal{R} [bpcu]	2, 3
Number of transmit antennas, N	2 ~ 5
Bandwidth, B_W [KHz]	1, 10, 10^2 , 10^3 , 10^4

$$P_{out} = \left[\Pr \left\{ \left(\sum_{l=1}^M \sum_{k=1}^{G_l} \bar{a}_{lk} \bar{b}_{lk} + \bar{c}_{su} \right)^2 < \frac{\sigma_U^2 \rho_{th}}{\left(1 - [\alpha_S^t]^2 + (\alpha_U^r)^2 \right) \rho_{th}} P_S \right\} \right]^N \quad (22)$$

where \bar{a}_{lk} and \bar{c}_{su} are, respectively, used to denote the channel magnitudes from an arbitrary antenna of S to the l^{th}/k^{th} and to U.

Let $\mathcal{X}_{lk} = \bar{a}_{lk} \bar{b}_{lk}$, $\mathcal{Y}_l = \sum_{k=1}^{G_l} \mathcal{X}_{lk}$, $\mathcal{Z} = \sum_{l=1}^M \mathcal{Y}_l$, and $\mathcal{T} = \mathcal{Z} + \bar{c}_{su}$. Then, (22) becomes

$$P_{out} = \left[\Pr \left\{ \mathcal{T}^2 < \frac{\sigma_U^2 \rho_{th}}{\left(1 - [\alpha_S^t]^2 + (\alpha_U^r)^2 \right) \rho_{th}} P_S \right\} \right]^N \quad (23)$$

From (23), the OP of the considered multi-RIS-assisted MW communications with ITH and with TAS is formulated as follows.

Theorem: Under the effects of ITH, the OP of the considered multi-RIS-assisted MW communications

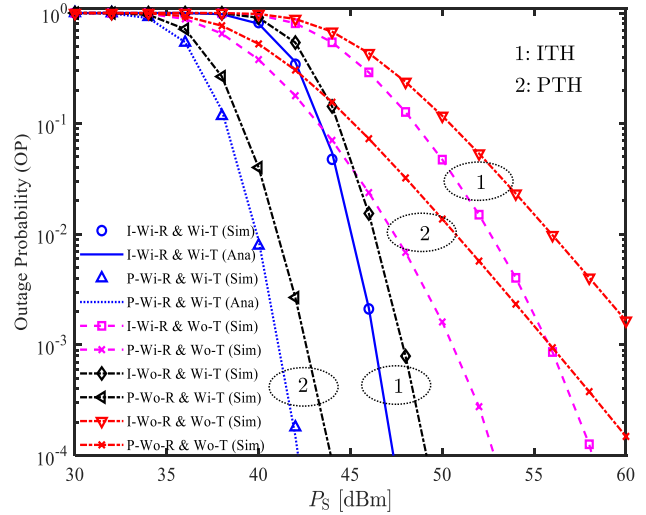


Fig. 2 The OP of the proposed communications versus transmit power in comparison with the OPs of relevant communications with $N = 5$ antennas, $\mathbf{x}_{RIS} = [20, 40, 60]$, $f_c = 50$ GHz, $\mathcal{R} = 3$ bpcu, $B_W = 10^4$ KHz, and $\alpha^2 = 0.1$

with TAS over realistic Nakagami- m channels when $1 - [(\alpha_S^t)^2 + (\alpha_U^r)^2] \rho_{th} > 0$ is given as

$$P_{out} = \sum_{n=0}^N \binom{N}{n} \frac{(-1)^n}{\Gamma^n \left(\frac{[\Delta_{\mathcal{T}}(1)]^2}{\Delta_{\mathcal{T}}(2) - [\Delta_{\mathcal{T}}(1)]^2} \right)} \times \Gamma^n \left(\frac{[\Delta_{\mathcal{T}}(1)]^2}{\Delta_{\mathcal{T}}(2) - [\Delta_{\mathcal{T}}(1)]^2}, \frac{\Delta_{\mathcal{T}}(1)}{\Delta_{\mathcal{T}}(2) - [\Delta_{\mathcal{T}}(1)]^2} \right) \times \sqrt{\frac{\sigma_U^2 \rho_{th}}{\left(1 - [(\alpha_S^t)^2 + (\alpha_U^r)^2] \rho_{th} \right) P_S}} \quad (24)$$

where $\binom{N}{n} = \frac{N!}{n!(N-n)!}$; $\Delta_{\mathcal{T}}(1)$ and $\Delta_{\mathcal{T}}(2)$ denote the first and second moments of \mathcal{T} , respectively, given in (45) and (46), respectively.⁶

⁶ It is essential to acknowledge that the computational complexity induced by multiple RISs and multiple antennas with ITH in multi-RIS-assisted MW communications is substantial. This complexity arises due to the considerably intricate formula derived in equation (24), surpassing the simplicity found in prior research [50, 54, 55]. Furthermore, this formula adeptly captures practical scenarios in multi-RIS-assisted MW communications with ITH and with TAS. The channel model, carrier frequency, and system parameters employed in this study are grounded in practical measurements, aligning with specific frequencies and path loss models recommended for 5G and B5G standards (as denoted in Eq. (14)). Notably, the carrier frequency normalization or exclusion of MW bands, as observed in previous works on RIS-aided wireless systems [50, 54, 55], renders their channel characteristics impractical and unsuitable for B5G networks.

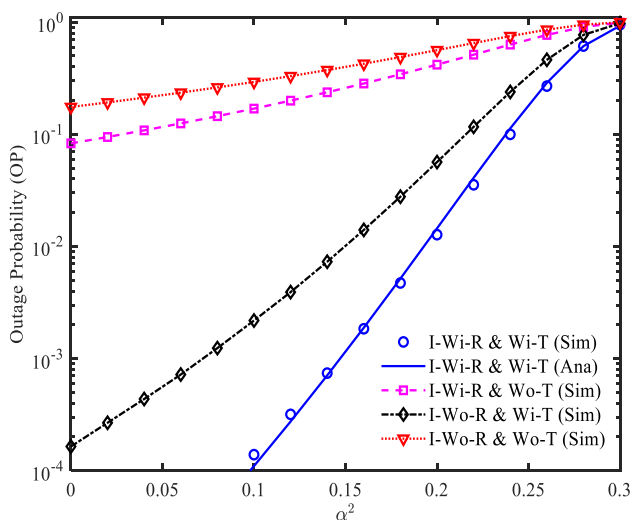


Fig. 3 The impacts of α^2 on the OP of the considered communications with $N = 5$ antennas, $P_S = 40$ dBm, $\mathbf{x}_{\text{RIS}} = [20, 40, 60]$, $f_c = 50$ GHz, $B_W = 10^4$ KHz, and $\mathcal{R} = 2$ bpcu

Proof Please refer to Appendix. □

3.2 System throughput

Besides the OP, the ST is an essential performance metric of wireless communications. In particular, the ST of the multi-RIS-assisted MW communications with ITH and with TAS is calculated as

$$ST = \mathcal{R}(1 - \mathcal{P}_{\text{out}}). \tag{25}$$

Substituting \mathcal{P}_{out} in (24) into (25), the ST is then formulated as

$$ST = \mathcal{R} \left[1 - \sum_{n=0}^N \binom{N}{n} \frac{(-1)^n}{\Gamma^n \left(\frac{[\Delta_{\mathcal{T}}(1)]^2}{\Delta_{\mathcal{T}}(2) - [\Delta_{\mathcal{T}}(1)]^2} \right)} \times \Gamma^n \left(\frac{[\Delta_{\mathcal{T}}(1)]^2}{\Delta_{\mathcal{T}}(2) - [\Delta_{\mathcal{T}}(1)]^2}, \frac{\Delta_{\mathcal{T}}(1)}{\Delta_{\mathcal{T}}(2) - [\Delta_{\mathcal{T}}(1)]^2} \sqrt{\frac{\sigma_{\text{U}}^2 \rho_{\text{th}}}{(1 - [(\alpha_{\text{S}}^t)^2 + (\alpha_{\text{U}}^t)^2] \rho_{\text{th}})} P_S} \right) \right]. \tag{26}$$

4 Numerical results and discussion

In this section, the behaviors of the considered communications are provided by using the obtained formulas. Monte-Carlo simulations using MATLAB software with 10^6 channel realizations are conducted to confirm the exactness of the obtained formulas. To clarify the great benefits of TAS, the performance of the considered communications with TAS is compared with that in the case without TAS. Moreover, the performance with RISs is also compared with that in the case without RISs. In addition,

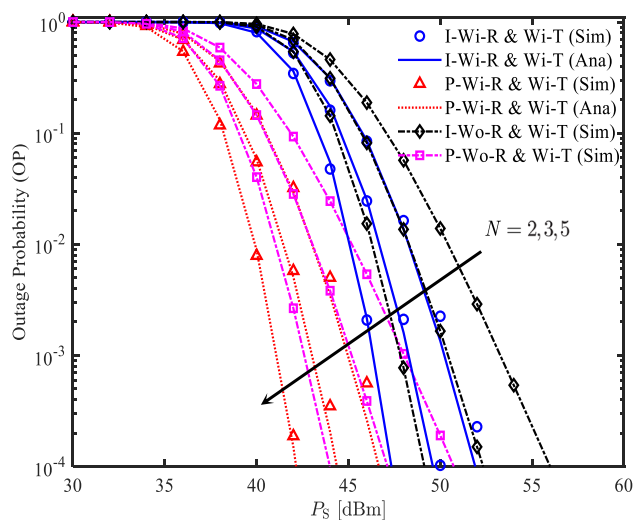


Fig. 4 The benefits of TAS in the considered communications with $N = 5$ antennas, $\mathbf{x}_{\text{RIS}} = [20, 40, 60]$, $f_c = 50$ GHz, $\mathcal{R} = 3$ bpcu, $B_W = 10^4$ KHz, and $\alpha^2 = 0.1$

the strong impacts of ITH are demonstrated when the performances with ITH and PTH are compared. In all investigated scenarios, the number of RISs is $M = 3$ and the shape parameters are $m_{su} = m_{a_i} = m_{b_i} = 2$. To derive σ_{U}^2 in (11), the thermal noise power density and noise figure are, respectively, set as $N_0 = -174$ dBm/Hz and $N_F = 10$ dBm while the bandwidth is changed. Similarly, to obtain Ω in (14), the antenna gains are fixed, i.e., $G_{\text{tx}} = G_{\text{rx}} = 5$ dB while f_c and d are varied depending on the specific scenarios.⁷ Moreover, the certain locations of S and U are fixed, i.e., $(\hat{x}_{\text{S}}, \hat{y}_{\text{S}}) = (0, 20)$ and $(\hat{x}_{\text{U}}, \hat{y}_{\text{U}}) = (100, 2)$ where (\hat{x}, \hat{y}) is the two-dimensional coordinates. Meanwhile, the RISs' positions are expressed via vector $\mathbf{x}_{\text{RIS}_s}$ and $\mathbf{y}_{\text{RIS}_s}$, e.g., $\mathbf{x}_{\text{RIS}_s} = [20, 40, 60]$ and $\mathbf{y}_{\text{RIS}_s} = [5, 10, 15]$ mean that $(\hat{x}_{\text{RIS}_1}, \hat{y}_{\text{RIS}_1}) = (20, 5)$, $(\hat{x}_{\text{RIS}_2}, \hat{y}_{\text{RIS}_2}) = (40, 10)$, and $(\hat{x}_{\text{RIS}_3}, \hat{y}_{\text{RIS}_3}) = (60, 15)$.⁸ The ITH levels at S and U are aggregated as $\alpha^2 = (\alpha_{\text{S}}^t)^2 + (\alpha_{\text{U}}^t)^2$. For reading conveniently, the notations in the figures are listed in Table 3 while the parameter settings are listed in Table 4.⁹

⁷ Besides considering antenna gains as constants, we can vary them to investigate the system behaviors. However, the antenna gains are often fixed because an increase in antenna gains will obviously improve the system performance [51, 61, 63].

⁸ From the specific coordinates, the distance d between two communication nodes is formulated as $d = \sqrt{(\hat{x}_i - \hat{x}_j)^2 + (\hat{y}_i - \hat{y}_j)^2}$ where $i, j = \text{S, U, RIS}_1, \text{RIS}_2, \text{RIS}_3$ and $i \neq j$.

⁹ As can be seen in Table 4, the system parameters are from the practical measurements and experiments. Therefore, the behaviors of the considered communications achieved in this section will deeply reflect the behaviors of the wireless communications being deployed in 5G networks. Meanwhile, many previous works such as [2, 43, 48, 50, 53] normalized the system parameters by setting $\Omega = 1$,

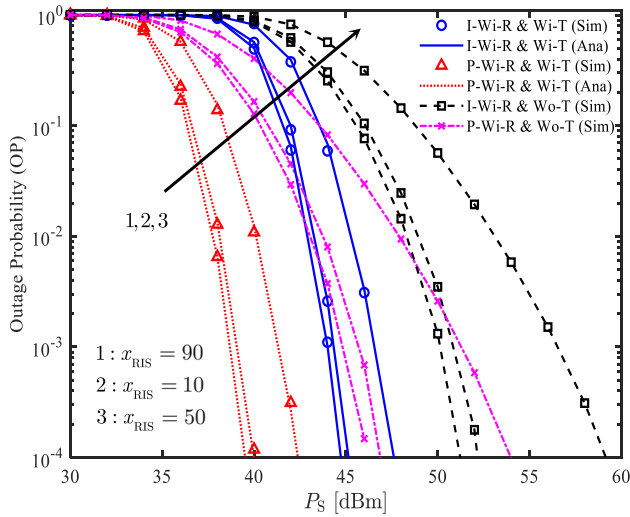


Fig. 5 The OP of the considered communications for different RISs' positions with $N = 5$ antennas, $f_c = 50$ GHz, $\mathcal{R} = 3$ bpcu, $B_W = 10^4$ KHz, and $\alpha^2 = 0.1$

Figure 2 depicts the OP of the considered communications (I-Wi-R & Wi-T) with $N = 5$ antennas, $\mathbf{x}_{\text{RIS}} = [20, 40, 60]$, $f_c = 50$ GHz, $\mathcal{R} = 3$ bpcu, $B_W = 10^4$ KHz, and $\alpha^2 = 0.1$. To demonstrate the benefits of using RISs and TAS as well as the strong impacts of ITH, the OPs of relevant communications are also provided for clear comparisons. Specifically, the OPs with PTH, with RISs, and with TAS (P-Wi-R & Wi-T), with ITH, with RISs, and without TAS (I-Wi-R & Wo-T), with PTH, with RISs, and without TAS (P-Wi-R & Wo-T), with ITH, without RISs, and with TAS (I-Wo-R & Wi-T), with PTH, without RISs, and with TAS (P-Wo-R & Wi-T), with ITH, without RISs, and without TAS (I-Wo-R & Wo-T), with PTH, without RISs, and without TAS (P-Wo-R & Wo-T) are detailedly presented in Fig. 2. The analytical curve of the OP of the considered communications is obtained by using (24). Moreover, (24) is also used to derive the analytical curve in the case of P-Wi-R & Wi-T by setting $\alpha^2 = 0$. Firstly, the effects of ITH are significant because the OPs in the cases of I-Wi-R & Wi-T, I-Wi-R & Wo-T, I-Wo-R & Wi-T, and I-Wo-R & Wo-T are greatly higher than those in the cases of P-Wi-R & Wi-T, P-Wi-R & Wo-T, P-Wo-R & Wi-T, and P-Wo-R & Wo-T, respectively. More specifically, to reach $\mathcal{P}_{\text{out}} = 10^{-4}$, the considered communications have to use $P_S = 47.5$ dBm while it is only 42.5 dBm in the case of P-Wi-R & Wi-T. In other words, P_S of the ITH communications has to be higher than that of PTH communications. Moreover, Fig. 2 demonstrates the great benefits of TAS

Footnote 9 (continued)

$\sigma^2 = 1$, and $f_c = 1$ Hz. Consequently, their results could not fully characterize the behaviors of practical wireless communications.

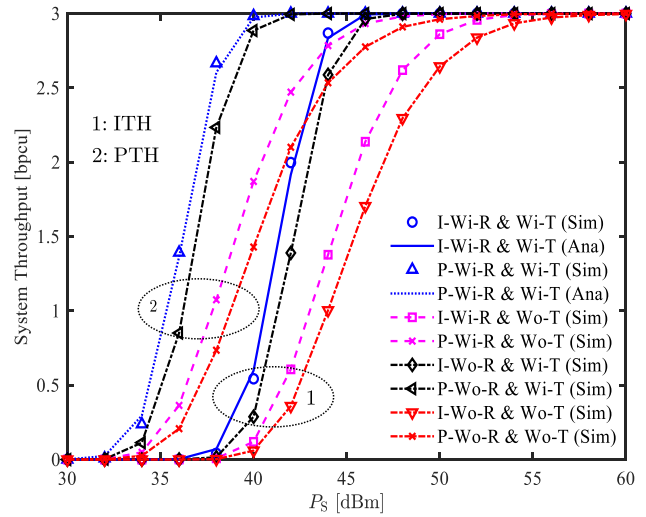


Fig. 6 The ST of the considered communications in comparison with STs of relevant communications for $N = 5$ antennas, $f_c = 50$ GHz, $\mathcal{R} = 3$ bpcu, $B_W = 10^4$ KHz, $\alpha^2 = 0.1$, and $\mathbf{x}_{\text{RIS}} = [20, 40, 60]$

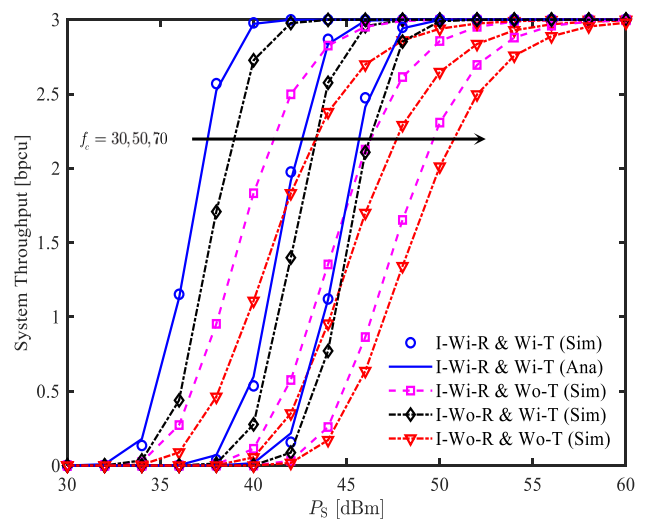


Fig. 7 The ST of the considered communications with different frequencies in MW bands for $N = 5$ antennas, $\mathcal{R} = 3$ bpcu, $B_W = 10^4$ KHz, $\alpha^2 = 0.1$, and $\mathbf{x}_{\text{RIS}} = [20, 40, 60]$

and RISs used in the MW communications. Particularly, with $\mathcal{P}_{\text{out}} = 10^{-4}$, the transmit powers are 47.5 dBm and 57 dBm corresponding to the cases I-Wi-R & Wi-T and I-Wi-R & Wo-T. In other words, the transmit power with TAS is 10 dBm lower than that without TAS. In addition, the OPs of I-Wi-R & Wi-T, P-Wi-R & Wi-T, I-Wi-R & Wo-T, and P-Wi-R & Wo-T (the MW communications with RISs) are, respectively, lower than those of I-Wo-R & Wi-T, P-Wo-R & Wi-T, I-Wo-R & Wo-T, and P-Wo-R & Wo-T (the MW communications without RISs). These results confirm the huge benefits of exploiting RISs and TAS in the proposed

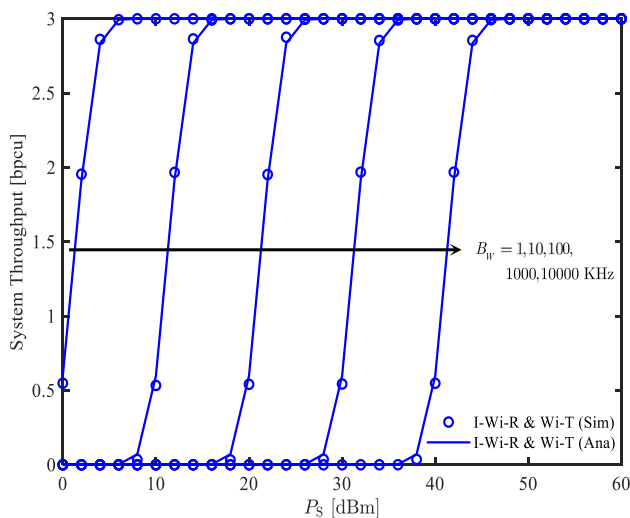


Fig. 8 The effects of bandwidth on the ST of the considered communications with $N = 5$ antennas, $\mathcal{R} = 3$ bpcu, $f_c = 50$ GHz, $\alpha^2 = 0.1$, and $\mathbf{x}_{\text{RIS}} = [20, 40, 60]$

communication. Thus, utilizing RISs greatly improves the OP performance of the MW communications even with ITH.

In Fig. 3, the OPs of ITH communications are illustrated where the ITH level α^2 is varied from 0 to 0.3. The system parameters are $N = 5$ antennas, $P_S = 40$ dBm, $\mathbf{x}_{\text{RIS}} = [20, 40, 60]$, $f_c = 50$ GHz, $B_W = 10^4$ KHz, and $\mathcal{R} = 2$ bpcu. It is worth noticing that when $\alpha^2 = 0$, the OPs of ITH communications become the OPs of PTH communications. It is clear in Fig. 3 that the impacts of α^2 are significant even with low values. In particular, when α^2 increases from 0 (PTH) to 0.06, the OPs of I-Wi-R & Wi-T, I-Wi-R & Wo-T, I-Wo-R & Wi-T, and I-Wo-R & Wo-T increase from 1.8×10^{-6} , 1.6×10^{-4} , 8.3×10^{-2} , and 1.8×10^{-1} to 1.9×10^{-5} , 7.2×10^{-4} , 1.2×10^{-1} , and 2.3×10^{-1} , respectively. Moreover, when α^2 increases, the OPs with TAS (I-Wi-R & Wi-T and I-Wo-R & Wi-T) are quickly increased while the OPs without TAS (I-Wi-R & Wo-T and I-Wo-R & Wo-T) are slowly increased. As a result, the effects of α^2 on the OPs with TAS are higher than those without TAS. In addition, the OP of I-Wo-R & Wi-T is dramatically lower than that of I-Wi-R & Wo-T. Once more, this characteristic serves as further evidence of the significant advantages associated with the TAS scheme employed in this article. In other words, the performance of classical communications without RISs and with TAS is dramatically higher than that of advanced communications with RISs and without TAS.

Figure 4 visually represents the advantages of TAS in the MW communications with and without RISs, with ITH and PTH. It is obvious that an increase in N greatly reduces the OPs of MW communications. Specifically, at $P_S = 46$ dBm, the OP of the considered communications (I-Wi-R & Wi-T) reduces from 8.2×10^{-2} to 2.5×10^{-2} and 2.1×10^{-3}

when N increases from 2 to 3 and 5. For a target of OP, i.e., $\mathcal{P}_{\text{out}} = 10^{-4}$, the transmit power of the considered communications are 52, 49.2, and 47.5 dBm corresponding to $N = 2, 3$, and 5. As a result, an increase in N can dramatically reduce the transmit power of S to obtain the specific target of OP. On the other hand, the characteristics of the OPs of P-Wi-R & Wi-T, I-Wo-R & Wi-T, and P-Wo-R & Wi-T are similar to those of the OP of the considered communications. Hence, employing a greater number of transmit antennas at S proves to be an efficient approach for enhancing the OP performance of the MW communications with ITH.

In Fig. 5, three positions of RISs are determined, i.e., $\mathbf{x}_{\text{RIS}} = [90, 90, 90]$ (case 1), $\mathbf{x}_{\text{RIS}} = [10, 10, 10]$ (case 2), and $\mathbf{x}_{\text{RIS}} = [50, 50, 50]$ (case 3). Unlike the RISs' positions in Figs. 2, 3, 4 where the three RISs have different positions ($\mathbf{x}_{\text{RIS}} = [20, 40, 60]$), the positions of the three RISs in Fig. 5 are similar in an investigated case. In other words, three RISs are grouped and located in a certain area. Among the three investigated areas, the OP in case 1 is the best while the OP in case 3 is the worst. Moreover, the OPs in cases 1 and 2 are nearly similar. It is noteworthy that the RISs are in the middle between S and U in case 3 while they are near to either S or U in cases 1 and 2. From these features, it can be concluded that the performance of the RISs-assisted MW communications can be dramatically improved by locating RISs near either the receiver or transmitter. Thus, it is better to deeply investigate the positions of RISs before deploying them in practice.

Figure 6 plots the ST of the considered communications in comparison with STs of relevant communications for $N = 5$ antennas, $f_c = 50$ GHz, $\mathcal{R} = 3$ bpcu, $B_W = 10^4$ KHz, $\alpha^2 = 0.1$, and $\mathbf{x}_{\text{RIS}} = [20, 40, 60]$. Herein, the analytical results of I-Wi-R & Wi-T and P-Wi-R & Wi-T are plotted by using (26). It is also noted that the ST of P-Wi-R & Wi-T is obtained by setting $\alpha^2 = 0$ in (26). Similar to the OP, the STs with ITH are greatly lower than the STs with PTH. This feature demonstrates a strong effect of ITH on the ST of the considered communications. In other words, the impact of ITH is substantial and should not be disregarded. More specifically, the considered communications have to use $P_S = 46$ dBm to reach the ST target of 3 bpcu. Meanwhile, it is only 40 dBm in the case of P-Wi-R & Wi-T. On the other hand, TAS can significantly enhance the ST of the considered communications. It is because without TAS, the I-Wi-R & Wo-T communications have to use $P_S = 54$ dBm to reach the ST target of 3 bpcu. As the results, TAS dramatically reduces the OP and considerably increases the ST of the considered communications.

In Fig. 7, the carrier frequency is varied, i.e., $f_c = 30, 50$, and 70 GHz while the other parameters are akin or comparable to those mentioned previously. Figure 7 clarifies the great impacts of f_c on the ST of the considered communications.

In particular, when f_c increases from 30 to 50 and 70 GHz, P_S has to increase from 38 to 44 and 48 dBm to reach the ST target of 3 bpcu. In other words, when f_c is 20 GHz higher, the transmit power has to increase about 4 dBm to keep the ST unchanging. Besides increasing the transmit power, an increase in N is also a good solution to indirectly take care of ITH and high carrier frequencies. As a result, it is important to use suitable frequencies in MW bands to avoid the performance reduction induced by the high carrier frequencies. When a higher carrier frequency has to be used, we should use a larger number of transmit antennas to keep similarly the ST of the considered communications.

Figure 8 illustrates the effects of bandwidth on the ST of the considered communications with $N = 5$ antennas, $\mathcal{R} = 3$ bpcu, $f_c = 50$ GHz, $\alpha^2 = 0.1$, and $\mathbf{x}_{\text{RIS}} = [20, 40, 60]$. Five bandwidths are determined, i.e., $B_W = 1, 10, 100, 1000$, and $10,000$ KHz. Since higher B_W leads to higher σ_U^2 (referred to (11)), the ST of the considered communications is greatly reduced when B_W increases. In particular, when B_W is 10 times higher, i.e., it increases from 1 to 10 KHz, the transmit power has to be increased 10 dBm to reach a target of 3 bpcu. As a result, when a wider bandwidth is used in the considered communications, the transmit power, the number of RISs/REs, and the number of transmit antennas should be higher for dramatically enhancing the system performance. These approaches can be considered as the low-cost solutions to improve the performance of the considered communications.

5 Conclusion

In this article, the practical scenarios of wireless communications were determined. Particularly, multi-RIS-assisted MW communications with ITH and with TAS were investigated. Besides ITH, the noise power and channel model are also computed from practice. Consequently, the considered communications can deeply reflect the behaviors of wireless systems used in B5G networks. The mathematical formulas of OP and ST of the considered communications were derived for obtaining the system behaviors. Then, many comparing scenarios were provided. Specifically, the performances are compared between with and without TAS, with and without RISs, and with and without ITH. Numerical results confirmed the big advantages of TAS and RISs in the considered multi-RIS-assisted MW communications with ITH. Therefore, by utilizing TAS with a larger number of transmit antennas, the effects of ITH can be greatly decreased. Besides this method, various effective solutions such as using a larger number of REs, choosing suitable positions of RISs, and utilizing appropriate frequencies and

bandwidths were deeply determined to gain more useful insights into the considered communication behaviors. Notably, optimization problems such as the positions of RISs, the numbers of REs in the RISs, and the optimal transmit power to reduce the impact of negative parameters and improve the system performance, should be continuously addressed. We leave them for future work.

Appendix

In this appendix, all mathematical derivations are detailedly presented to derive the OP formula of the considered communications with TAS and ITH in (24).

Since \bar{c}_{su} is the single channel from S to U, its h th moment can be computed as [64]

$$\Delta_{\bar{c}_{su}}(h) \triangleq \mathbb{E}\{(\bar{c}_{su})^h\} = \int_0^\infty y^h f_{\bar{c}_{su}}(y) dy. \tag{27}$$

After using (13), (27) becomes

$$\Delta_{\bar{c}_{su}}(h) = \frac{\Gamma(m_{su} + h/2)}{\Gamma(m_{su})} \left(\frac{m_{su}}{\Omega_{su}}\right)^{-h/2}. \tag{28}$$

From (28), the 1st and 2nd moments of \bar{c}_{su} are, respectively, given as

$$\Delta_{\bar{c}_{su}}(1) = \frac{\Gamma(m_{su} + 1/2)}{\Gamma(m_{su})} \sqrt{\frac{\Omega_{su}}{m_{su}}}, \tag{29}$$

$$\Delta_{\bar{c}_{su}}(2) = \Omega_{su}. \tag{30}$$

Since $\mathcal{X}_{lk} = \bar{a}_{lk} \bar{b}_{lk}$, its PDF is [65]

$$f_{\mathcal{X}_{lk}}(\rho) = \int_0^\infty \frac{1}{y} f_{\bar{a}_{lk}}\left(\frac{\rho}{y}\right) f_{\bar{b}_{lk}}(y) dy. \tag{31}$$

Utilizing (13), (31) is now expressed as

$$f_{\mathcal{X}_{lk}}(\rho) = \frac{4}{\Gamma(m_{b_l})\Gamma(m_{a_l})} \left(\frac{m_{b_l}}{\Omega_{b_l}}\right)^{m_{b_l}} \left(\frac{m_{a_l}}{\Omega_{a_l}}\right)^{m_{a_l}} \alpha^{2m_{a_l}-1} \times \int_0^\infty y^{2m_{b_l}-2m_{a_l}-1} \exp\left(-\frac{\rho^2 m_{a_l}}{\Omega_{a_l} y^2} - \frac{m_{b_l} y^2}{\Omega_{b_l}}\right) dy. \tag{32}$$

Applying [66, Eq. (3.478.4)], (32) becomes

$$f_{\mathcal{X}_{lk}}(\rho) = \frac{4}{\Gamma(m_{a_l})\Gamma(m_{b_l})} \left(\frac{m_{a_l} m_{b_l}}{\Omega_{a_l} \Omega_{b_l}}\right)^{\frac{m_{a_l} + m_{b_l}}{2}} \rho^{m_{a_l} + m_{b_l} - 1} \times \mathcal{K}_{m_{b_l} - m_{a_l}}\left(2\rho \sqrt{\frac{m_{a_l} m_{b_l}}{\Omega_{a_l} \Omega_{b_l}}}\right). \tag{33}$$

Based on (33), the h th moment of \mathcal{X}_{lk} is calculated as

$$\Delta_{\mathcal{X}_{lk}}(h) \triangleq \mathbb{E}\{\mathcal{X}_{lk}^h\} = \int_0^\infty y^h f_{\mathcal{X}_{lk}}(y) dy. \tag{34}$$

After utilizing [66, Eq. (6.561.16)], (34) becomes

$$\Delta_{\mathcal{X}_{lk}}(h) = \left(\frac{m_{a_l} m_{b_l}}{\Omega_{a_l} \Omega_{b_l}}\right)^{\frac{-h}{2}} \times \frac{\Gamma(m_{a_l} + h/2) \Gamma(m_{b_l} + h/2)}{\Gamma(m_{a_l}) \Gamma(m_{b_l})}. \tag{35}$$

Based on (35), the specific moments of $\Delta_{\mathcal{X}_{lk}}$ can be straightforwardly derived, i.e.,

$$\Delta_{\mathcal{X}_{lk}}(1) = \sqrt{\frac{\Omega_{a_l} \Omega_{b_l}}{m_{a_l} m_{b_l}}} \times \frac{\Gamma(m_{a_l} + 1/2) \Gamma(m_{b_l} + 1/2)}{\Gamma(m_{a_l}) \Gamma(m_{b_l})}, \tag{36}$$

$$\Delta_{\mathcal{X}_{lk}}(2) = \frac{\Omega_{a_l} \Omega_{b_l}}{m_{a_l} m_{b_l}} \times \frac{\Gamma(m_{a_l} + 1) \Gamma(m_{b_l} + 1)}{\Gamma(m_{a_l}) \Gamma(m_{b_l})} = \Omega_{a_l} \Omega_{b_l}. \tag{37}$$

From the above moments, the CDF of \mathcal{X}_{lk} is obtained as [51]

$$F_{\mathcal{X}_{lk}}(\rho) \approx \frac{1}{\Gamma\left(\frac{[\Delta_{\mathcal{X}_{lk}}(1)]^2}{\Delta_{\mathcal{X}_{lk}}(2) - [\Delta_{\mathcal{X}_{lk}}(1)]^2}\right)} \gamma\left(\frac{[\Delta_{\mathcal{X}_{lk}}(1)]^2}{\Delta_{\mathcal{X}_{lk}}(2) - [\Delta_{\mathcal{X}_{lk}}(1)]^2}, \frac{\Delta_{\mathcal{X}_{lk}}(1)\rho}{\Delta_{\mathcal{X}_{lk}}(2) - [\Delta_{\mathcal{X}_{lk}}(1)]^2}\right). \tag{38}$$

It is because $\mathcal{Y}_l = \sum_{k=1}^{G_l} \mathcal{X}_{lk}$, its CDF is formulated as [67]

$$F_{\mathcal{Y}_l}(\rho) \approx \frac{1}{\Gamma\left(\frac{[\Delta_{\mathcal{X}_{lk}}(1)]^2 G_l}{\Delta_{\mathcal{X}_{lk}}(2) - [\Delta_{\mathcal{X}_{lk}}(1)]^2}\right)} \gamma\left(\frac{[\Delta_{\mathcal{X}_{lk}}(1)]^2 G_l}{\Delta_{\mathcal{X}_{lk}}(2) - [\Delta_{\mathcal{X}_{lk}}(1)]^2}, \frac{\Delta_{\mathcal{X}_{lk}}(1)\rho}{\Delta_{\mathcal{X}_{lk}}(2) - [\Delta_{\mathcal{X}_{lk}}(1)]^2}\right). \tag{39}$$

Now, the h th moment of \mathcal{Y}_l is formulated [68]

$$\Delta_{\mathcal{Y}_l}(h) \triangleq \mathbb{E}\{\mathcal{Y}_l^h\} = \sum_{h_1=0}^h \sum_{h_2=0}^{h_1} \dots \sum_{h_{G_l-1}=0}^{h_{G_l-2}} \binom{h}{h_1} \binom{h_1}{h_2} \dots \binom{h_{G_l-2}}{h_{G_l-1}} \times \Delta_{\mathcal{X}_{l1}}(t - h_1) \Delta_{\mathcal{X}_{l2}}(h_1 - h_2) \dots \Delta_{\mathcal{X}_{lG_l}}(h_{G_l-1}). \tag{40}$$

On the other hand, since $\mathcal{Z} = \sum_{l=1}^M \mathcal{Y}_l$, its h th moment is also formulated as

$$\Delta_{\mathcal{Z}}(h) \triangleq \mathbb{E}\{\mathcal{Z}^h\} = \sum_{h_1=0}^h \sum_{h_2=0}^{h_1} \dots \sum_{h_{M-1}=0}^{h_{M-2}} \binom{h}{h_1} \binom{h_1}{h_2} \dots \binom{h_{M-2}}{h_{M-1}} \times \Delta_{\mathcal{Y}_1}(t - h_1) \Delta_{\mathcal{Y}_2}(h_1 - h_2) \dots \Delta_{\mathcal{Y}_M}(h_{M-1}). \tag{41}$$

Now, based on (35), (40), and (41), the specific moments of \mathcal{Z} can be derived, i.e.,

$$\Delta_{\mathcal{Z}}(1) = \sum_{l=1}^M \sum_{k=1}^{G_l} \Delta_{\mathcal{X}_{lk}}(1), \tag{42}$$

$$\Delta_{\mathcal{Z}}(2) = \sum_{l=1}^M \left[\sum_{k=1}^{G_l} \Delta_{\mathcal{X}_{lk}}(2) + 2 \sum_{k=1}^{G_l} \Delta_{\mathcal{X}_{lk}}(1) \sum_{k'=k+1}^{G_l} \Delta_{\mathcal{X}_{lk'}}(1) \right] + 2 \sum_{l=1}^M \left[\sum_{k=1}^{G_l} \Delta_{\mathcal{X}_{lk}}(1) \right] \sum_{l'=l+1}^M \left[\sum_{k=1}^{L_{l'}} \Delta_{\mathcal{X}_{l'k}}(1) \right], \tag{43}$$

where $\Delta_{\mathcal{X}_{lk}}(1)$ and $\Delta_{\mathcal{X}_{lk}}(2)$ are, respectively, given in (36) and (37).

Then, the h th moment of $\mathcal{T} = \mathcal{Z} + \bar{c}_{su}$ can be formulated as

$$\Delta_{\mathcal{T}}(h) \triangleq \mathbb{E}\{(\mathcal{Z} + \bar{c}_{su})^h\} = \mathbb{E}\left\{ \sum_{i=0}^h \binom{h}{i} \bar{c}_{su}^i \mathcal{Z}^{h-i} \right\} = \sum_{i=0}^h \binom{h}{i} \Delta_{\bar{c}_{su}}(i) \Delta_{\mathcal{Z}}(h - i). \tag{44}$$

Based on (44), the specific moments of \mathcal{T} can be derived, i.e.,

$$\Delta_{\mathcal{T}}(1) = \Delta_{\mathcal{Z}}(1) + \Delta_{\bar{c}_{su}}(1), \tag{45}$$

$$\Delta_{\mathcal{T}}(2) = \Delta_{\mathcal{Z}}(2) + \Delta_{\bar{c}_{su}}(2) + 2\Delta_{\mathcal{Z}}(1)\Delta_{\bar{c}_{su}}(1). \tag{46}$$

Now, the CDF of \mathcal{T} can be obtained from its moments [51], thus, we obtain

$$F_{\mathcal{T}}(\rho) = \frac{1}{\Gamma\left(\frac{[\Delta_{\mathcal{T}}(1)]^2}{\Delta_{\mathcal{T}}(2) - [\Delta_{\mathcal{T}}(1)]^2}\right)} \gamma\left(\frac{[\Delta_{\mathcal{T}}(1)]^2}{\Delta_{\mathcal{T}}(2) - [\Delta_{\mathcal{T}}(1)]^2}, \frac{\Delta_{\mathcal{T}}(1)\rho}{\Delta_{\mathcal{T}}(2) - [\Delta_{\mathcal{T}}(1)]^2}\right) = 1 - \frac{1}{\Gamma\left(\frac{[\Delta_{\mathcal{T}}(1)]^2}{\Delta_{\mathcal{T}}(2) - [\Delta_{\mathcal{T}}(1)]^2}\right)} \Gamma\left(\frac{[\Delta_{\mathcal{T}}(1)]^2}{\Delta_{\mathcal{T}}(2) - [\Delta_{\mathcal{T}}(1)]^2}, \frac{\Delta_{\mathcal{T}}(1)\rho}{\Delta_{\mathcal{T}}(2) - [\Delta_{\mathcal{T}}(1)]^2}\right). \tag{47}$$

Then, the OP from (23) is expressed as

$$\mathcal{P}_{\text{out}} = \left[\Pr\left\{ \mathcal{T}^2 < \frac{\sigma_U^2 \rho_{\text{th}}}{\left(1 - [(\alpha_S^t)^2 + (\alpha_U^r)^2\right] \rho_{\text{th}}}\right) \mathcal{P}_S \right\} \right]^N = \left[\Pr\left\{ \mathcal{T} < \sqrt{\frac{\sigma_U^2 \rho_{\text{th}}}{\left(1 - [(\alpha_S^t)^2 + (\alpha_U^r)^2\right] \rho_{\text{th}}}\right) \mathcal{P}_S} \right\} \right]^N = \left[F_{\mathcal{T}}\left(\sqrt{\frac{\sigma_U^2 \rho_{\text{th}}}{\left(1 - [(\alpha_S^t)^2 + (\alpha_U^r)^2\right] \rho_{\text{th}}}\right) \mathcal{P}_S} \right) \right]^N. \tag{48}$$

Applying (47), (48) is solved as

$$\mathcal{P}_{\text{out}} = \left[F_{\mathcal{T}} \left(\sqrt{\frac{\sigma_{\text{U}}^2 \rho_{\text{th}}}{\left(1 - [(\alpha_{\text{S}}^{\text{t}})^2 + (\alpha_{\text{U}}^{\text{r}})^2\right) \rho_{\text{th}}}} \right) P_{\text{S}} \right)^N \quad (49)$$

$$= \left[1 - \frac{1}{\Gamma\left(\frac{[\Delta_{\mathcal{T}}(1)]^2}{\Delta_{\mathcal{T}}(2) - [\Delta_{\mathcal{T}}(1)]^2}\right)} \right.$$

$$\times \Gamma\left(\frac{[\Delta_{\mathcal{T}}(1)]^2}{\Delta_{\mathcal{T}}(2) - [\Delta_{\mathcal{T}}(1)]^2}, \frac{\Delta_{\mathcal{T}}(1)}{\Delta_{\mathcal{T}}(2) - [\Delta_{\mathcal{T}}(1)]^2} \right.$$

$$\left. \left. \sqrt{\frac{\sigma_{\text{U}}^2 \rho_{\text{th}}}{\left(1 - [(\alpha_{\text{S}}^{\text{t}})^2 + (\alpha_{\text{U}}^{\text{r}})^2\right) \rho_{\text{th}}}} \right) P_{\text{S}} \right)^N. \quad (50)$$

Utilizing the binomial theorem, the OP formula of the considered communications with TAS is derived as (24) in Theorem. The proof is now complete. \square

References

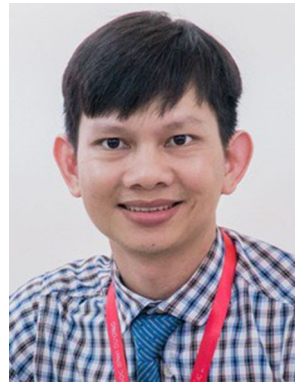
- Altin, G., & Arslan, I. (2022). Joint transmit and receive antenna selection for spatial modulation systems using deep learning. *IEEE Communications Letters*, 26(9), 2077–2080.
- Nguyen, B. C., Tran, X. N., Nguyen, L. V., & Dung, L. T. (2020). On the performance of full-duplex spatial modulation MIMO system with and without transmit antenna selection under imperfect hardware conditions. *IEEE Access*, 8, 185218–18531.
- Mohamed, A., Bai, Z., Pang, K., He, B., Ma, Y., & Kwak, K. S. (2023). Transmit antenna subset selection in cooperative SM-MIMO vehicular system. *IEEE Communications Letters*, 27(7), 1744–1748.
- Badrudeen, A. A., Leow, C. Y., & Won, S. (2022). Hybrid beamformer exploiting multistream per user transmission for millimeter-wave NOMA communications. *IEEE Access*, 10, 23074–23085.
- Zhu, L., Xiao, Z., Xia, X., & Wu, D. O. (2019). Millimeter-wave communications with non-orthogonal multiple access for B5G/6G. *IEEE Access*, 7, 116123–116132.
- Sharma, M. K., Kumar, M., & Saini, J. P. (2021). Design and analysis of a compact UWB-MIMO antenna with improved isolation for UWB/WLAN applications. *Wireless Personal Communications*, 119(4), 2913–2928.
- Kumar, R., Sharma, M., Matta, L., Kaur, P., Saluja, N., Malhotra, S., Singh, M., Saini, G. S., & Singh, S. (2023). Mutual coupling reduction techniques for UWB - MIMO antenna for band notch characteristics: A comprehensive review. *Wireless Personal Communications*, 131(2), 1207–1247.
- Saxena, G., Jain, P., & Awasthi, Y. K. (2020). High diversity gain MIMO-antenna for UWB application with WLAN notch band characteristic including human interface devices. *Wireless Personal Communications*, 112(1), 105–121.
- Kumar, J. P., & Karunakar, G. (2020). Compact UWB-MIMO triple notched antenna for isolation reduction. *Wireless Personal Communications*, 115(3), 2113–2125.
- Saritha, V., & Chandrasekhar, C. (2021). A study and review on frequency band notch characteristics in reconfigurable MIMO-UWB antennas. *Wireless Personal Communications*, 118(4), 2631–2661.
- Addepalli, T., & Anitha, V. R. (2022). Parametric analysis of compact UWB-MIMO antenna with improved isolation using parasitic reflectors and protruded ground strips. *Wireless Personal Communications*, 123(3), 2209–2225.
- Wu, L., Lyu, H., & Yu, H. (2019). A novel compact UWB-MIMO antenna with quintuple notched-band characteristics. *Wireless Personal Communications*, 108(3), 1827–1840.
- Jayant, S., & Srivastava, G. (2021). Compact 4 x 4 proximity coupled microstrip fed UWB stepped slot MIMO antenna having triple band rejection. *Wireless Personal Communications*, 119(4), 3719–3734.
- Babu, K. V., & Anuradha, B. (2021). Design of UWB MIMO antenna to reduce the mutual coupling using defected ground structure. *Wireless Personal Communications*, 118(4), 3469–3484.
- Kumar, R., & Pazare, N. (2016). A printed semi-circular disc UWB MIMO/diversity antenna with cross shape slot stub. *Wireless Personal Communications*, 91(1), 277–291.
- Abdelraheem, A., & Abdalla, M. A. (2018). Bi-directional UWB MIMO antenna for superior spatial diversity, and/or multiplexing MIMO performance. *Wireless Personal Communications*, 101(3), 1379–1394.
- Indoonundon, M., & Fowdur, T. P. (2022). Enhancing the error performance of 5G new radio using hierarchical and statistical QAM. *Wireless Personal Communications*, 125(2), 1951–1972.
- Gupta, M., Kang, A. S., & Sharma, V. (2022). Comparative study on implementation performance analysis of simulink models of cognitive radio based GFDM and UPMC techniques for 5G wireless communication. *Wireless Personal Communications*, 126(1), 135–165.
- Feng, C., Shen, W., An, J., & Hanzo, L. (2022). Joint hybrid and passive RIS-assisted beamforming for mmwave MIMO systems relying on dynamically configured subarrays. *IEEE Internet Things Journal*, 9(15), 13913–13926.
- Banar, M., Mohammadi, A., & Kazemi, M. (2022). Characterization of mmwave full-duplex cloud-radio access network (C-RAN) with RRH selection for 5G and beyond. *Physics Communications*, 52, 101693.
- Peng, Z., Pan, C., Zhou, G., Ren, H., Jin, S., Popovski, P., Schober, R., & You, X. (2023). Two-stage channel estimation for RIS-aided multiuser mmwave systems with reduced error propagation and pilot overhead. *IEEE Transactions on Signal Processing*, 71, 3607–3622.
- Nguyen, K. K., Masaracchia, A., Sharma, V., Poor, H. V., & Duong, T. Q. (2022). RIS-assisted UAV communications for IoT with wireless power transfer using deep reinforcement learning. *IEEE Journal of Selected Topics in Signal Processing*, 16(5), 1086–1096.
- Lin, Y., Jin, S., Matthaiou, M., & You, X. (2022). Channel estimation and user localization for IRS-assisted MIMO-OFDM systems. *IEEE Transactions on Wireless Communications*, 21(4), 2320–2335.
- Yu, Z., Han, Y., Matthaiou, M., Li, X., & Jin, S. (2022). Statistical CSI-based design for RIS-assisted communication systems. *IEEE Wireless Communications Letter*, 11(10), 2115–2119.
- Nguyen, K. K., Khosravirad, S. R., da Costa, D. B., Nguyen, L. D., & Duong, T. Q. (2022). Reconfigurable intelligent surface-assisted multi-UAV networks: Efficient resource allocation with deep reinforcement learning. *IEEE Journal of Selected Topics in Signal Processing*, 16(3), 358–368.
- Wu, M., Guo, K., Li, X., Nauman, A., An, K., & Wang, J. (2024). Optimization design in RIS-assisted integrated satellite-UAV-served 6G IoT: A deep reinforcement learning approach. *IEEE Internet Things Magazine*, 7(1), 12–18.
- Khan, W. U., Mahmood, A., Sheemar, C. K., Lagunas, E., Chatzinas, S., & Ottersten, B. E. (2024). Reconfigurable intelligent surfaces for 6G non-terrestrial networks: Assisting connectivity from the sky. *IEEE Internet Things Magazine*, 7(1), 34–39.

28. Rahim, M., Nguyen, T., Kaddoum, G., & Do, T. N. (2024). Multi-IRS-aided terahertz networks: Channel modeling and user association with imperfect CSI. *IEEE Open Journal of the Communications Society*, 5, 836–855.
29. Xu, B., Zhou, T., Tao, X., Xu, T., & Wang, Y. (2022). Ergodic capacity analysis for relay-RIS system under three-dimensional channel model. *IEEE Communications Letters*, 26(10), 2292–2296.
30. Mensi, N., & Rawat, D. B. (2022). On the performance of partial RIS selection vs. partial relay selection for vehicular communications. *IEEE Transactions on Vehicular Technology*, 71(9), 9475–9489.
31. Wen, Y., Chen, G., Fang, S., Wen, M., Tomasin, S., & Renzo, M. D. (2024). RIS-assisted UAV secure communications with artificial noise-aware trajectory design against multiple colluding curious users. *IEEE Transactions on Information Forensics and Security*, 19, 3064–3076.
32. Ismail, M. I., Shaheen, A. M., Fouda, M. M., & Alwakeel, A. S. (2024). RIS-assisted integrated sensing and communication systems: Joint reflection and beamforming design. *IEEE Open Journal of the Communications Society*, 5, 908–927.
33. He, J., Jiang, F., Keykhosravi, K., Kokkonniemi, J., Wymeersch, H., & Juntti, M. J. (2022). Beyond 5G RIS mmwave systems: Where communication and localization meet. *IEEE Access*, 10, 68 075–68 084.
34. Gao, P., Lian, L., & Yu, J. (2022). Wireless area positioning in RIS-assisted mmwave systems: Joint passive and active beamforming design. *IEEE Signal Processing Letters*, 29, 1372–1376.
35. Li, R., Guo, B., Tao, M., Liu, Y., & Yu, W. (2022). Joint design of hybrid beamforming and reflection coefficients in RIS-aided mmwave MIMO systems. *IEEE Transactions on Communications*, 70(4), 2404–2416.
36. Katwe, M., Singh, K., Clerckx, B., & Li, C. (2022). Rate-splitting multiple access and dynamic user clustering for sum-rate maximization in multiple RISs-aided uplink mmwave system. *IEEE Transactions on Communications*, 70(11), 7365–7383.
37. Tam, D. T., Van Vinh, N., & Nguyen, B. C. (2022). Improving the performance of multi-IRS aided millimeter-wave communication systems by transmit antenna selection. *Physics Communications*, 56, 101957.
38. Tang, W., Chen, M. Z., Chen, X., Dai, J. Y., Han, Y., Renzo, M. D., Zeng, Y., Jin, S., Cheng, Q., & Cui, T. J. (2021). Wireless communications with reconfigurable intelligent surface: Path loss modeling and experimental measurement. *IEEE Transactions on Wireless Communications*, 20(1), 421–439.
39. Rezaei, A., Khalili, A., Jalali, J., Shafiei, H., & Wu, Q. (2022). Energy-efficient resource allocation and antenna selection for IRS-assisted multicell downlink networks. *IEEE Wireless Communications Letters*, 11(6), 1229–1233.
40. He, J., Yu, K., Shi, Y., Zhou, Y., Chen, W., & Letaief, K. B. (2022). Reconfigurable intelligent surface assisted massive MIMO with antenna selection. *IEEE Transactions on Wireless Communications*, 21(7), 4769–4783.
41. Abdullah, Z., Chen, G., Lambotaran, S., & Chambers, J. A. (2022). Low-complexity antenna selection and discrete phase-shifts design in IRS-assisted multiuser massive MIMO networks. *IEEE Transactions on Vehicular Technology*, 71(4), 3980–3994.
42. Xu, C., An, J., Bai, T., Sugiura, S., Maunder, R.G., Yang, L.L., Di Renzo, M. & Hanzo, L., (2023). Antenna selection for reconfigurable intelligent surfaces: A transceiver-agnostic passive beamforming configuration. *IEEE Transactions on Wireless Communications* 1–19.
43. Nguyen, L. V., Nguyen, B. C., Tran, X. N., & Dung, L. T. (2020). Transmit antenna selection for full-duplex spatial modulation multiple-input multiple-output system. *IEEE Systems Journal*, 14(4), 4777–4785.
44. Tran, P. T., Nguyen, B. C., Hoang, T. M., & Nguyen, T. N. (2023). On performance of low-power wide-area networks with the combining of reconfigurable intelligent surfaces and relay. *IEEE Transactions on Mobile Computing*, 22(10), 6086–6096.
45. Al-Ahmadi, A. (2024). Knowledge distillation based deep learning model for user equipment positioning in massive MIMO systems using flying reconfigurable intelligent surfaces. *IEEE Access*, 12, 20679–20691.
46. Nerini, M., Shen, S., & Clerckx, B. (2024). Closed-form global optimization of beyond diagonal reconfigurable intelligent surfaces. *IEEE Transactions on Wireless Communications*, 23(2), 1037–1051.
47. Schenk, T. (2008). *RF imperfections in high-rate wireless systems: Impact and digital compensation*. Springer Science & Business Media.
48. Papazafeiropoulos, A. K., Sharma, S. K., Ratnarajah, T., & Chatzinothas, S. (2018). Impact of residual additive transceiver hardware impairments on Rayleigh-product MIMO channels with linear receivers: Exact and asymptotic analyses. *IEEE Transactions on Communications*, 66(1), 105–118.
49. Tam, D. T., Nguyen, B. C., Van Vinh, N., et al. (2022). Outage and throughput performance of hybrid RISs-relay-aided-wireless systems with imperfect transceiver hardware. *AEU - International Journal of Electronics and Communications*, 157, 154425.
50. Boulogeorgos, A. A., & Alexiou, A. (2020). How much do hardware imperfections affect the performance of reconfigurable intelligent surface-assisted systems? *IEEE Open Journal of the Communications Society*, 1, 1185–1195.
51. Tran, P. T., Nguyen, B. C., Hoang, T. M., Le, X. H., & Nguyen, V. D. (2022). Exploiting multiple RISs and direct link for performance enhancement of wireless systems with hardware impairments. *IEEE Transactions on Communications*, 70(8), 5599–5611.
52. Guo, K., & An, K. (2022). On the performance of RIS-assisted integrated satellite-UAV-terrestrial networks with hardware impairments and interference. *IEEE Wireless Communications Letters*, 11(1), 131–135.
53. Dai, J., Zhu, F., Pan, C., Ren, H., & Wang, K. (2022). Statistical CSI-based transmission design for reconfigurable intelligent surface-aided massive MIMO systems with hardware impairments. *IEEE Wireless Communications Letters*, 11(1), 38–42.
54. Atapattu, S., Fan, R., Dharmawansa, P., Wang, G., Evans, J. S., & Tsiftsis, T. A. (2020). Reconfigurable intelligent surface assisted two-way communications: Performance analysis and optimization. *IEEE Transactions on Communications*, 68(10), 6552–6567.
55. Nguyen, T. N., Thang, N. N., Nguyen, B. C., Hoang, T. M., & Tran, P. T. (2023). Intelligent-reflecting-surface-aided bidirectional full-duplex communication system with imperfect self-interference cancellation and hardware impairments. *IEEE Systems Journal*, 17(1), 1352–1362.
56. Nguyen, B. C., Hoang, T. M., Dung, L. T., & Kim, T. (2021). On performance of two-way full-duplex communication system with reconfigurable intelligent surface. *IEEE Access*, 9, 81274–81285.
57. Xiu, Y., Zhao, J., Sun, W., Renzo, M. D., Gui, G., Zhang, Z., & Wei, N. (2021). Reconfigurable intelligent surfaces aided mmwave NOMA: Joint power allocation, phase shifts, and hybrid beamforming optimization. *IEEE Transactions on Wireless Communications*, 20(12), 8393–8409.
58. Jokinen, M., Kursu, O., Tervo, N., Pärssinen, A., & Leinonen, M. E. (2024). Over-the-air phase calibration methods for 5G mmW antenna array transceivers. *IEEE Access*, 12, 28057–28070.
59. Zhi, K., Pan, C., Ren, H., Chai, K. K., & El-kashlan, M. (2022). Active RIS versus passive RIS: Which is superior with the same power budget? *IEEE Communications Letters*, 26(5), 1150–1154.
60. Wu, Q., & Zhang, R. (2020). Beamforming optimization for wireless network aided by intelligent reflecting surface with discrete

- phase shifts. *IEEE Transactions on Communications*, 68(3), 1838–1851.
61. Björnson, E., Özdogan, Ö., & Larsson, E. G. (2019). Intelligent reflecting surface versus decode-and-forward: How large surfaces are needed to beat relaying? *IEEE Wireless Communications Letters*, 9(2), 244–248.
 62. Ibrahim, H., Tabassum, H., & Nguyen, U. T. (2021). Exact coverage analysis of intelligent reflecting surfaces with nakagami-m channels. *IEEE Transactions on Vehicular Technology*, 70(1), 1072–1076.
 63. Yildirim, I., Uyrus, A., & Basar, E. (2021). Modeling and analysis of reconfigurable intelligent surfaces for indoor and outdoor applications in future wireless networks. *IEEE Transactions on Communications*, 69(2), 1290–1301.
 64. Goldsmith, A. (2005). *Wireless communications*. Cambridge University Press.
 65. Phan, V.-D., Nguyen, B. C., Hoang, T. M., Nguyen, T. N., Tran, P. T., Minh, B. V., & Voznak, M. (2022). Performance of cooperative communication system with multiple reconfigurable intelligent surfaces over nakagami-m fading channels. *IEEE Access*, 10, 9806–9816.
 66. Jeffrey, A., & Zwillinger, D. (2007). *Table of integrals, series, and products*. Academic Press.
 67. Galappaththige, D. L., Kudathanthirige, D., & Amarasuriya, G. (2020). Performance analysis of distributed intelligent reflective surface aided communications. In *IEEE Global Communications Conference, GLOBECOM. IEEE*, (pp. 1–6).
 68. da Costa, D. B., Ding, H., & Ge, J. (2011). Interference-limited relaying transmissions in dual-hop cooperative networks over nakagami-m fading. *IEEE Communications Letters*, 15(5), 503–505.

Publisher's Note Springer Nature remains neutral with regard to jurisdictional claims in published maps and institutional affiliations.

Springer Nature or its licensor (e.g. a society or other partner) holds exclusive rights to this article under a publishing agreement with the author(s) or other rightsholder(s); author self-archiving of the accepted manuscript version of this article is solely governed by the terms of such publishing agreement and applicable law.



physical layer security, and NOMA.

Nguyen Van Vinh was born in Binh Dinh, Viet Nam, in 1984. He received the B.E. degree in Computer Science from Nha Trang University, Vietnam, in 2008. In 2015, he received a Master's degree in Computer Science from University of Transport and Communications, Vietnam. He is currently a lecturer at the Department of Information Assurance (IA), FPT University, Ho Chi Minh City, Vietnam. His research interests are wireless communication in 5G, networking, cybersecurity,